Influence of the Anode Length on the Neutron Emission of a 50 J Plasma Focus: Modeling and Experiment

Alejandro Clausse, Leopoldo Soto, and Ariel Tarifeño-Saldivia

***Abstract*— A comprehensive set of electric data measured in a small plasma focus (PF) device of 50 J correlated with the corresponding neutron emissions is taken as the base for developing a semiempirical model of the current sheet dynamics and the neutron yield. The model is able to explain the dependence of the neutron yield with the pressure and anode length with good accuracy, and suggests a physical interpretation of the drive parameter commonly used in PF design.**

***Index Terms*— Anode, fusion neutrons, modeling, plasma focus (PF), plasma pinch.**

I. Introduction

A PLASMA focus (PF) is a type of pinch discharge in which a high-pulsed voltage is applied to a low-pressure gas, a few millibar, between coaxial cylindrical electrodes, generating a short-duration high-density plasma region in the axis (pinch) [1], [2]. This discharge reproduces a scenario of high energy density, intense beams of charged and neutral particles, plasma jets, plasma filaments, shock waves, and radiation emission. Thus, PF devices have become facilities for fundamental and applied research related to fusion, neutron production, hard X-ray, high brightness soft X-ray production, and astrophysical phenomena [1]. There is a great amount of research devoted to the physical mechanisms of neutron production, namely, thermonuclear and beam-target fusion [3]–[6]. Moreover, PF discharges can be viewed as self-scale z-pinches, for devices operating at a wide energy range (from <1 J to MJ) have practically the same value of ion density, magnetic field, plasma sheath velocity, Alfvén speed, and thermal energy per particle [2], [7]. On the other hand, a new generation of low energy, fast, and compact plasma foci [8]–[22] are attracting increasing interest for their potential applications and portability as neutron and X-ray sources. Comparing with isotopic neutron sources, PF have unique qualities as sources of X-ray/neutron pulses, emitting only on operator demand, with low risk of radiation contamination and low cost of operation and maintenance. PF devices are also interesting for industrial applications [23], ranging from tailored soft X-ray sources [24]–[26], and soft X-ray microlithography [27] to hard X-ray introspective imaging of metallic pieces [28]–[31], neutron production and applications [10], [12]–[14], [32], [33], detection of substances [34], plasma thrusters [35], materials testing [36], nanotechnologies [37], among others.

Although PF devices have been studied in many laboratories throughout the world, the physical processes underlying their behavior are still a matter of controversy. It is known for example that an optimal filling pressure value exists for any device at which maximum neutron yield is emitted; however, there is still no conclusive agreement regarding the reasons for the existence of such optimum pressure. Another common feature is the shot-to-shot fluctuations under apparently identical operating conditions (electrodes geometry, voltage, pressure); and it is not clear why this is so. Finally, whether the neutrons are produced by thermal plasma, a beam of high-energy deuterons, or a mix of both, is still a debated question. Hence, much systematic work on these devices is still needed to reach a proper understanding of their functioning, and further take advantage of their multiple potential applications. Several types of models were developed in the past to assist the design of PF devices. Currently, the kinematics of the current sheath can be calculated with quite sophisticated detail with the restructuring sheath model based in variable finite elements, which reproduced very precisely the shape evolution of the sheath and the thermodynamics of the shock wave [38], [44], [45]. On the other hand, lumped-parameters models were applied with excellent results, providing fast tools to assess the dynamic features of PF. Lee *et al.* [6] proposed a model based in the snow-plow approximation of the Magneto Hydro Dynamics equations, which was further extended to the simulation of different types of devices.

The modeling of the pinch dynamics and the corresponding radiation emission is probably the most complicated and

Manuscript received July 13, 2014; revised November 6, 2014; accepted November 20, 2014. Date of publication January 1, 2015; date of current version February 6, 2015. This work was supported in part by the Programa de Investigación Asociativa-National Scientific and Technical Research Council, Chile, under Grant ACT-1115, and in part by the Proyectos de Investigación Científica y Tecnológica under Grant 2697.

A. Clausse is with the National Atomic Energy Commission, National Scientific and Technical Research Council, National University of Central Buenos Aires, Tandil 7000, Argentina (e-mail: clausse@exa.unicen.edu.ar).

L. Soto is with the Comisión Chilena de Energía Nuclear, Santiago 8340701, Chile, the Center for Research and Applications in Plasma Physics and Pulsed Power, P4, Santiago 7600713, Chile, and also with the Departamento de Ciencias Físicas, Facultad de Ciencias Exactas, Universidad Andrés Bello, Santiago 7550162, Chile (e-mail: lsoto@cchen.cl).

Tarifeño-Saldivia was with the Comisión Chilena de Energía Nuclear, Santiago 8340701, Chile, and also with the Center for Research and Applications in Plasma Physics and Pulsed Power, P4, Santiago 7600713, Chile. He is now with the Instituto de Física Corpuscular, Consejo Superior de Investigaciones Científicas, Universidad de Valencia, Valence 46010, Spain (e-mail: atarisal@gmail.com).

Color versions of one or more of the figures in this paper are available online at http://ieeexplore.ieee.org.

Digital Object Identifier 10.1109/TPS.2014.2376412

controversial part of PF theory. González *et al.* [48], [49] applied a lumped-parameter model based on the method of weighted residuals to explain the experimental neutron and X-ray production of numerous devices. Moreover, this model successfully predicted the evolution of the internal density of the pinch of a low-energy PF [19]. The concept from which this family of models was derived was presented in the liminal papers [42] and [43], leading to a purely algebraic model capable of explaining the relation of the neutron production with the gas-filling pressure and the geometry of the device, based in the thermonuclear component of the fusion reaction.

The main inconvenient in developing models of PF discharges is the shortage of complete experimental data to validate the models and determine appropriate efficient parameters. In effect, although there is a large number of data available in the open literature, most of them lack the complete diagnostic required by the benchmarking of numerical models. In particular, careful measurements and correlations of the current and timing of the pinch with the neutron emissions are seldom available. Moreover, it is difficult to find complete electric and neutronic diagnostics performed in the same device varying the geometry of electrodes [47]. The latter is actually rather troublesome to perform in large facilities, whereas in small devices where these changes are easier to plan, neutron yields are often too small to measure with sufficient precision.

In this paper, a comprehensive set of electric data measured in a small PF device of 50 J correlated with the corresponding neutron emissions is used to develop an extended model of PF operation. The data is an extended set of results from the experimental study presented in [20] and [46], where a new technique was especially developed to measure neutron pulses of low intensity [39], [40]. The model is able to explain the dependence of the neutron yield with the pressure and anode length, and suggests a physical interpretation of the empirical scaling laws commonly used in PF design.

II. Experiment

The experiments were performed at the Chilean Nuclear Energy Commission in the compact PF device PF-50 J, which is a very-low energy PF device operating in the range of tens of Joules designed to produce fast discharges (quarter of period ∼150 ns) in H2 or D2 [11], [12], [18]–[20], [38]. The capacitor bank consisted in four units (40 nF, 20 nH, each) connected in parallel around a spark-gap. The characteristics parameters of the device are: 1) 160 nF equivalent capacitance; 2) ∼40 nH total inductance in short circuit; 3) 150 ns first quarter of period; 4) 25–35-kV charge voltage; 5) energy $E \sim 50$–70 J; and 6) 50–60-kA peak current in short circuit. The overall size and weight is 25 cm × 25 cm × 50 cm and 50 kg.

The electrode configuration corresponding to the data used in this paper is schematically shown in Fig. 1. Fig. 2 shows a photograph of the capacitor bank and the electrode configuration, which consists of a central stainless steel anode of 3-mm radius (r_1) and a hollow of 4.5-mm diameter. The hollow has a linear depth of 18 mm. The insulator is made

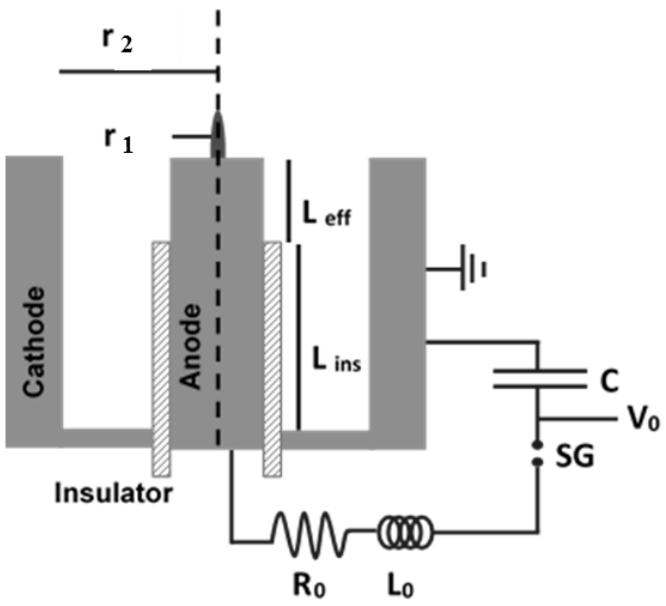

Fig. 1. Electrode configuration and circuit. Anode radius: r_1. Internal cathode radius: r_2. Effective anode length: L_{eff}. Effective insulator length: L_{ins}. Capacitance: C. Total inductance at short circuit on the insulator: L_o. Total resistance at short circuit on the insulator: R_o. Spark-gap: SG. Charging voltage: V_o.

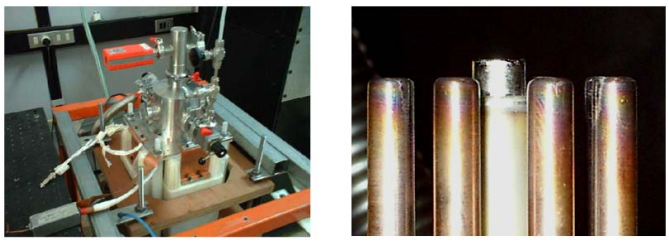

Fig. 2. General view of PF-50 J (left), electrode's configuration (right). The diameter of the anode (at center) is 6 mm.

from alumina, 1/4″ inner diameter, and 3/8″ outer diameter. The insulator effective length is $L_{\text{ins}} = 24.5$ mm. The cathode is made from six stainless steel 4.5-mm diameter rods, 34-mm effective length, uniformly spaced on a circumference of 8.75-mm radius, thus the inner cathode radius is $r_2 = 6.5$ mm. A field distortion element was placed at the base of the cathode plate next to the insulator bottom edge. This element is made from a 0.5-mm-thick copper strip, and its purpose is to help preionizing the gas volume close to the insulator. The discharge chamber is filled with D2. The capacitor bank is charged at 28.5 kV (∼65 J) and the discharge is initiated by self-breakdown of the spark-gap. The repetition rate of the discharge is ∼0.4–0.5 Hz.

The anode voltage and circuit current derivative are monitored using a calibrated resistive divider and a Rogowski coil, respectively. The circuit current is obtained by numerical integration of the signal of the current derivative. The neutron yield diagnostics consisted in two detection systems based on 3He proportional counters tubes moderated by paraffin wax, one located on the axis and the other located radially [39]. The 3He detection systems were calibrated in efficiency only, using as reference a standard isotopic fast-neutron source (^{252}Cf). Neutron yield is obtained by means of

TABLE I

LIST OF EXPERIMENTAL RESULTS. THE AVERAGE OF EACH PARAMETER IS REPORTED WITH THE UNCERTAINTY GIVEN BY THE STANDARD ERROR OF THE AVERAGE. AVERAGES OF THE NEUTRON PRODUCTION OF ALL SHOTS OF EACH RUN AND THE BEST 10% WITH HIGHER NEUTRON EMISSION ARE LISTED. THE LATTER IS USED TO COMPARE WITH THE THEORETICAL MODEL.

L_{eff}	p	#shots	I_p	δI_p	I_{max}	δI_{max}	t_p	δt_p	Y	δY	Y	δY
(mm)	(mbar)	-	(kA)		(kA)		(ns)		Best 10%		All shots	
3.7	7.5	9	47.4	0.3	48	0.3	150.2	1.1	1782	104	1530	253
3.7	8.5	10	48.1	0.2	49	0.2	156.4	1	2688	143	2406	366
3.7	9	8	47.9	0.5	49	0.4	158.2	1.2	5121	410	4897	970
3.7	9.5	11	49.5	0.5	50.8	0.5	158	0.9	5539	533	5819	1251
3.7	10	10	49.8	0.5	51.8	0.3	163.6	1.7	5484	308	4078	1159
3.7	10.9	9	47.2	1.1	50.9	0.9	175.3	2.1	4048	567	4551	1441
3.7	12	10	42	0.5	48.6	0.3	190.9	1.6	868	129	1050	298
4.6	5.6	9	50.6	0.3	50.9	0.3	140.2	1.2	2053	280	2313	649
4.6	6.3	10	50.5	0.3	51	0.2	148.4	2.1	4205	256	3531	862
4.6	7.1	11	49.8	0.3	51.1	0.3	158	1.1	8332	914	7192	1857
4.6	7.3	10	49.3	0.5	51.3	0.5	164.4	1.7	6085	322	4644	960
4.6	7.6	10	47.6	0.5	50.1	0.3	166.2	1.3	10208	1013	8150	2299
4.6	8.2	10	46.6	0.4	51	0.3	176.8	1.7	7972	641	4360	1575
4.6	9.3	10	42.9	0.5	50.9	0.2	191.8	1.3	1710	134	1752	252
4.6	10.3	7	40.6	0.8	50.5	0.4	198.2	1.8	1580	138	2202	550
5.5	4.3	11	49.3	0.2	49.6	0.2	139.9	1.8	4697	417	3673	1104
5.5	5	10	48.3	0.2	49.9	0.2	157.8	1	6056	738	5530	1682
5.5	5.4	11	49	0.2	50.2	0.1	158.3	1.1	8206	907	7451	2056
5.5	5.7	10	48.3	0.3	50.3	0.3	160.2	1.2	11689	1034	11488	2876
5.5	5.9	11	47	0.3	49.4	0.1	170.4	1.6	6228	406	4455	1129
5.5	6.2	11	46.6	0.7	50	0.3	170.4	2.3	8701	832	7375	1863
5.5	6.5	10	45.7	0.6	50	0.2	178.6	3	8764	774	7757	1778
5.5	7	10	42.6	0.6	49.7	0.2	192.6	1.7	1851	175	1303	406
5.5	7.8	5	38	0.3	49.1	0.1	206.1	1.4	522	46	516	138
6.3	3	10	49.8	0.3	50.2	0.3	128.8	1.8	1859	183	1431	319
6.3	3.8	10	49.6	0.8	50.1	0.8	142.2	2.1	373	69	2288	622
6.3	4.5	12	47.2	0.6	48.9	0.5	154.4	1.6	3793	265	3288	745
6.3	5	10	47.9	0.7	50.9	0.3	165	2.6	7697	569	7901	1592
6.3	5.3	10	47.6	0.5	51	0.4	170.3	1.5	13049	653	12881	1830
6.3	5.5	11	47	0.7	49.6	0.5	166.3	1.8	9231	818	9897	2262
6.3	6	10	46	0.5	50.1	0.4	174.9	1.8	6614	525	5633	1336
6.3	6.4	11	43.3	0.4	50.7	0.2	189	1.5	2038	320	2082	592
6.3	7	9	32.3	9	51.2	0.3	225.9	27.8	843	101	937	187

a methodology especially developed to measure low yield neutron pulses [39], [40].

A series of experimental runs were conducted using four different anode configurations, with corresponding effective lengths L_{eff} of 3.7, 4.6, 5.5, and 6.3 mm. The filling gas pressure was varied in the range 2–12 mbar. For each run, a sample of ∼150 shots was acquired and the electrical signals of 10–15 shots were saved. Fig. 3 shows an electrical signal acquired at 5.3 mbar and $L_{\text{eff}} = 6.3$ mm, showing the definition of the pinch timing (t_p), the circuit current at the pinch (I_p), and maximum current ($I_{\max}$).

The list of the experimental results for the complete data sample is shown in Table I. In this table, the average magnitudes are together with the uncertainties given by the standard error of the average. The neutron production in Table I is listed for each effective anode length and pressure. Average of the neutron yield taken over all the shots of the sample and the 10% of the shots with higher neutron emission are given. The latter is typically referred in the literature as representative of the good shots [20] and was used to compare with the theoretical model.

III. MODEL OF THE PINCH TIME

In [42] and [43], the pinch time can be related to the filling pressure and the effective anode length using a

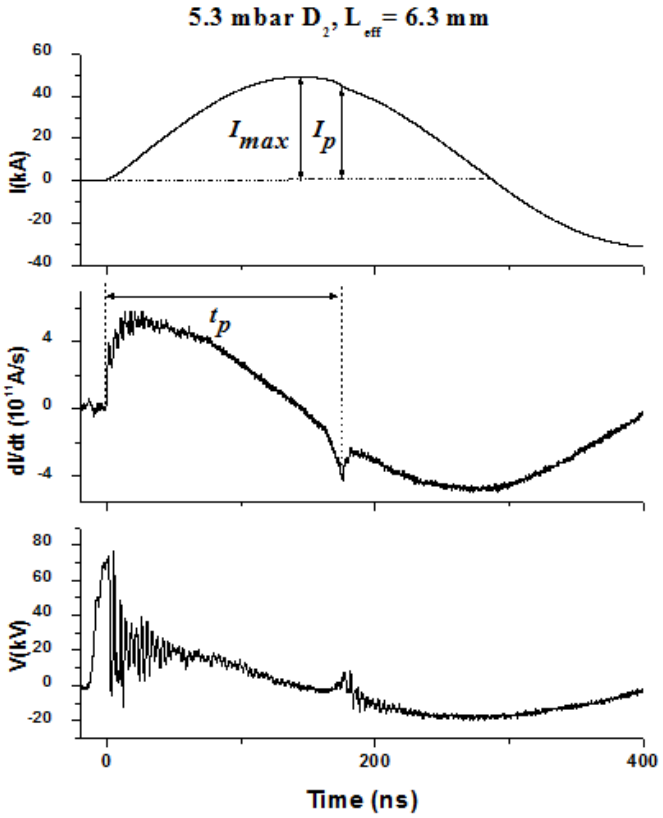

Fig. 3. Electrical signals. Current I, current derivative dI/dt, and voltage V. Time to pinch t_p, the circuit current at the pinch I_p, and the maximum circuit current $I_{\max}$.

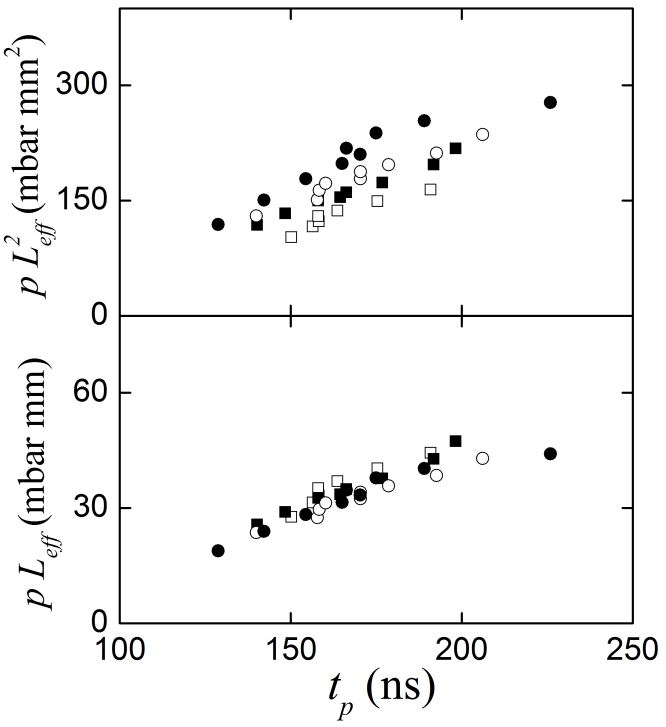

Fig. 4. Relation between the pressure, the anode length, and the pinching time. L_{eff}(mm) = 3.7 (□), 4.6 (■), 5.5 (◯), 6.3 (●).

1-D lumped model. Accordingly, the temporal evolution of the position of the barycenter of the sheet, z, moving axially, and the instantaneous charge of the capacitor Q are given by

$$\frac{d}{dt}\left(mz\frac{dz}{dt}\right) = \frac{1}{2}l\left(\frac{dQ}{dt}\right)^2 \tag{1}$$

$$\frac{d}{dt}\left[(L+lz)\frac{dQ}{dt}\right] + \frac{Q}{C} = 0 \tag{2}$$

where C is the capacity of the bank, L_o is the external inductance, m and $l = (\mu_o/2\pi)\ln(r_2/r_1)$ are the mass and inductance per unit length of the gun, and μ_o is the vacuum permeability (4×10^{-7} J/mA2). The right-hand-side of (1) is the Lorentz force acting on the current sheet. If lz is sufficiently small, variations of the total inductance can be neglected, and the pinch time t_p, and current I_p satisfy

$$L_{\text{eff}}^2 = \frac{lQ_o^2}{4m}\left(t_p^2\omega^2 - \sin^2\omega t_p\right) \tag{3}$$

$$I_p = Q_o\omega\ \sin\omega t_p \tag{4}$$

where Q_o is the initial charge of the capacitor, L_{eff} is the effective anode length (i.e., total length minus insulator length), and the natural angular frequency of the system is

$$\omega = \sqrt{L_o + lL_{\text{eff}}}. \tag{5}$$

Equations (1)–(5) are bound by several assumptions that make a fair approximation when the length of the anode is much larger than the interelectrode gap, the external inductance is much larger than the gun inductance, the current sheet keeps the same shape during most of the discharge time, among other conditions. Nevertheless, (3) can be used to provide a theoretical support for semiempirical correlations that account for deviations from the model hypothesis. Accordingly, since m is proportional to the filling pressure, one would expect that the experimental data followed a relation

$$pL_{\text{eff}}^{\alpha} = f(t_p) \tag{6}$$

where alpha is an effective parameter. Fig. 4 shows the plot of the experimental data in the plane $(pL_{\text{eff}}^{\alpha}, t_p)$. It can be seen that data sets of different L_{eff} do not show a unique trend for $\alpha = 2$, as it would be the case if the model assumptions hold [see the exponent of L_{eff} in (3)]. However, as the lower graphic shows, a power $\alpha = 1$ produces a single trend for all the data. Likewise, the dependence on the pinch time deviates from (4), which can be attributed primarily to the temporal variation of the current-sheet inductance. A general function that considers these features was accordingly adopted here, namely

$$r_1 L_{\text{eff}} = \frac{lQ_o^2}{4m}(\omega t_p)^{1.4}. \tag{7}$$

The mass per unit length m is related to the filling pressure p by the equation of state of the filling gas

$$m = \xi_A \frac{\pi\left(r_2^2 - r_1^2\right)\ m_i\, p}{kT_o} \tag{8}$$

where m_i is the deuteron mass, k is the Boltzmann constant, T_o is the ambient temperature (20 °C), and ξ_A is a coefficient that accounts for shape corrections.

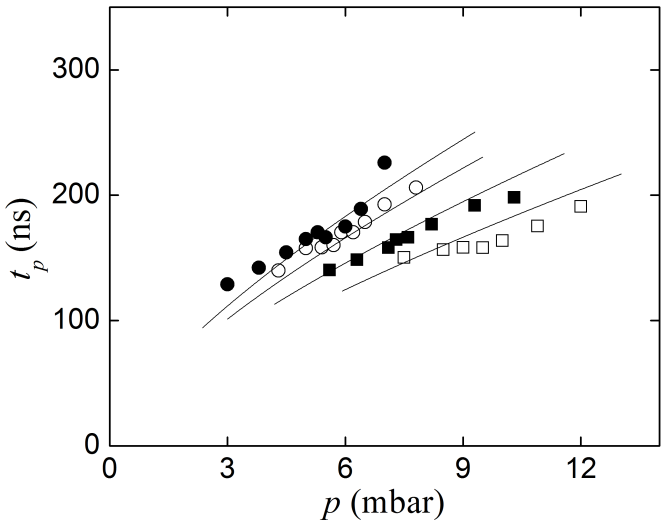

Fig. 5. Pressure dependence of the pinching time. L_{eff}(mm) = 3.7 (□), 4.6 (■), 5.5 (◯), 6.3 (●). The curves correspond to (7) and (8) with $\xi_A = 2.3$.

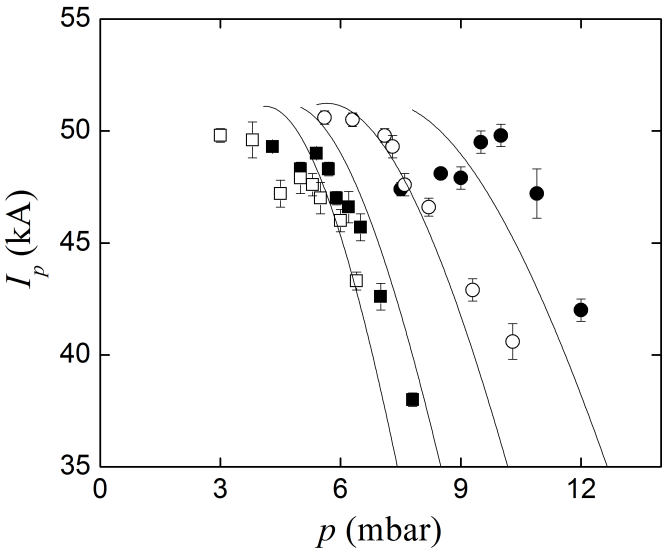

Fig. 6. Pressure dependence of the pinch current. L_{eff}(mm) = 3.7 (□), 4.6 (■), 5.5 (◯), 6.3 (●). The curves correspond to (4), (7), and (8) with $\xi_A = 2.3$.

Fig. 5 compares the correlation given by (7) and (8) with the measured dependence of the pinching time with pressure for different anode length. The optimum value calculated for the shape coefficient ξ_A is 2.3. The pinch current also depends on the pressure, as shown in Fig. 6. The general behavior can be appreciated in the map shown in Fig. 7, where it can be seen that the experimental range corresponds to a section of the ridge-like dependence of the pinch current with the pressure and anode length.

IV. Model of the Neutron Yield

It is possible to estimate the neutron yield coming from the focus assuming that it is proportional to the thermonuclear

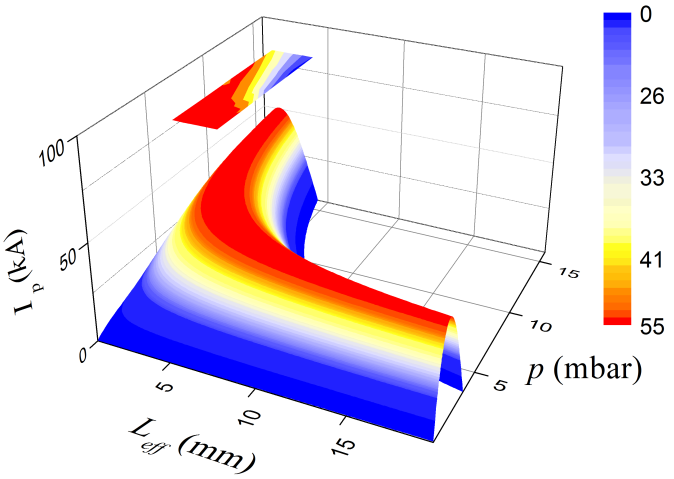

Fig. 7. Dependence of the pinch current with the filling pressure and the effective anode length. The contour map with the interpolation of the experimental data is shown in the upper projection for comparison.

component [42]. The total yield production in a plasma pinch column of volume V where fusion conditions are produced during a pulse Δt can be estimated as

$$Y = \frac{1}{4}\int_{\Delta t} n^2 \langle \sigma v \rangle V dt \tag{9}$$

where n is the average number of deuterons per unit volume and $\langle \sigma v \rangle$ is the effective thermonuclear cross section. Following the analysis described in [43], the Bennett equilibrium conditions can be used as an educated assessment of the relation between the pinch parameters. Accordingly

$$\langle \sigma v \rangle = A\theta^{-2/3} e^{(-\theta^{-1/3})} \tag{10}$$

$$\Delta t = \frac{\pi r_p}{2}\sqrt{\frac{3m_i}{2kT_B}} \tag{11}$$

where $A = 3.31\,10^{-23}$ m^3/s, $\theta = T_B/7.65 \times 10^{10}$ K, T_B is the Bennett temperature, given by

$$T_B = \frac{h}{k}\frac{\mu_o}{16\pi}\frac{I_p^2}{N} \tag{12}$$

where h is the pinch length and r_p is the effective pinch radius, related to the temperature assuming the pinch is adiabatic, that is

$$r_p = r_s \theta^{-3/4}. \tag{13}$$

The number of deuterons participating in the reaction is estimated as a fraction ξ_R of the deuterons contained in the cylindrical volume between the anode and the axis, that is

$$N = \xi_R \frac{\rho_o}{m_i} h\pi r_1^2 \tag{14}$$

where ρ_o is the density of the filling gas, related to the filling pressure p, and temperature T_o by the equation of state

$$\rho_o = \frac{pm_i}{kT_o}. \tag{15}$$

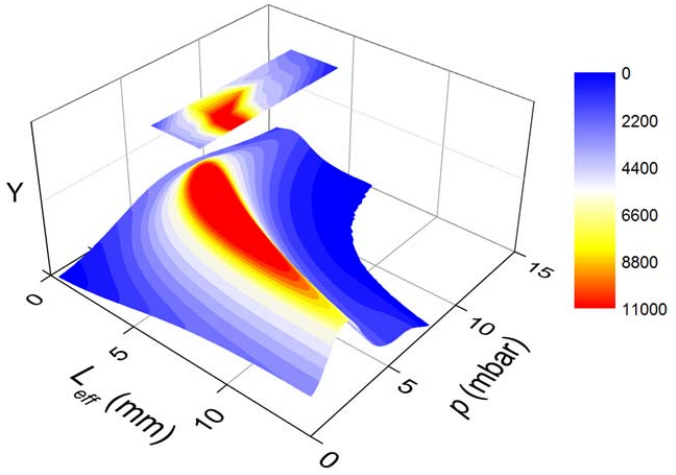

Fig. 8. Dependence of the neutron yield on the effective anode length and deuterium pressure ($h = r_1$). The contour map with the interpolation of the experimental data is shown in the upper projection for comparison.

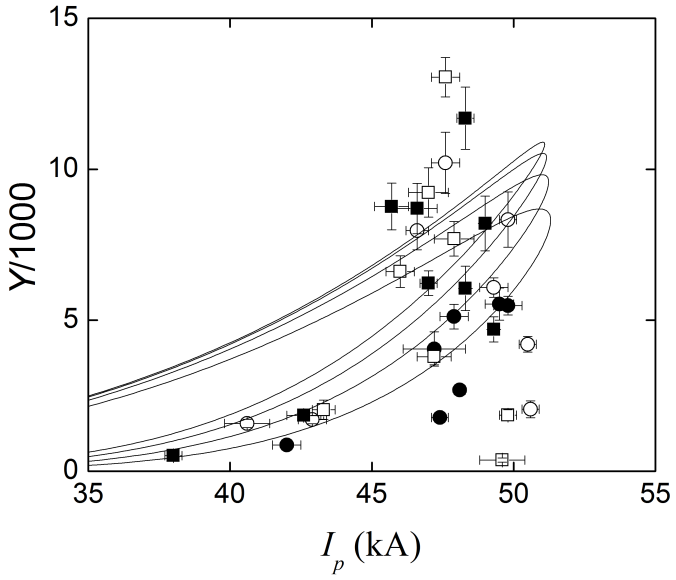

Fig. 9. Experimental (points) and numerical (curves) neutron yield dependence on the pinch current ($h = r_1$). L_{eff}(mm) = 3.7 (□), 4.6 (■), 5.5 (◯), 6.3 (●).

The parameters r_s (adiabatic reference) and ξ_R (reactive fraction of the pinch mass) were calibrated with the experimental data, resulting $r_s = 5.25 \times 10^{-7}$ m and $\xi_R = 0.012$. By combining (12), (14), and (15) the neutron yield Y can be related to the filling pressure and the effective anode length. As can be observed in Fig. 8, there is an optimum region of operation with the shape of a banana. The experimental region matches the wider section of the optimum region in the numerical calculation. The neutron yield is also coupled to the pinch current, although this dependence is multivalued as can be observed in Fig. 9. In this projection there is a general agreement with the experiments, but unfortunately the data is too scattered to discriminate with the anode length.

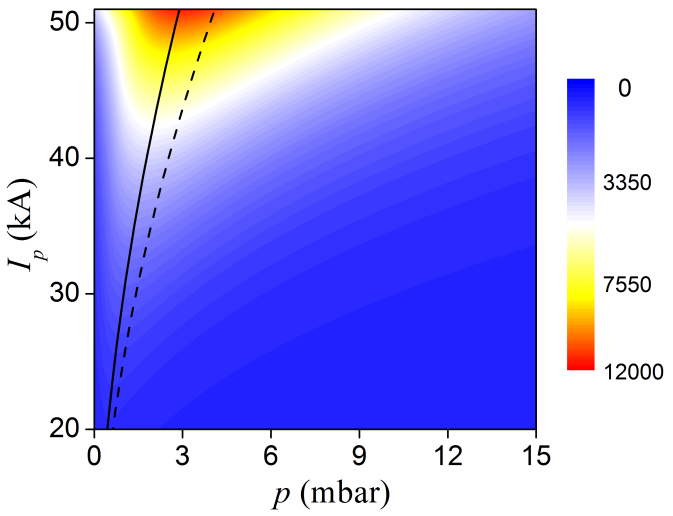

Fig. 10. Neutron yield as function of the pinch current and pressure ($h = r_1$). The solid and dashed curves correspond to $I_p/(r_1\sqrt{p}) = 91$ and 77 kA/cm mbar$^{1/2}$, respectively.

The maximum neutron yield in the model is reached when the dimensionless pinch temperature estimated in the Bennett equilibrium is equal to $\theta = (4/29)^3$ and the pinch current coincident with the maximum achievable current, that is $I_p = I_{\max} = \omega Q_o$ [42], [43]. Introducing this condition in (12), (14), and (15) lead to the following criterion for optimal design and operation:

$$\frac{I_{\max}^2}{p r_1^2} = \frac{(4\pi)^2}{\mu_o} \frac{(4/29)^3}{\theta_o} \xi_R \tag{16}$$

where θ_o is the dimensionless temperature of the filling gas, which at room temperature is $\sim 4 \times 10^{-9}$. The left-hand-side of (16) is the square of the drive parameter, $I_{\max}/(r_1\sqrt{p})$, which has been empirically correlated in the past with good performances of PF devices when its value lies $\sim$77 kA/cm mbar$^{1/2}$ [2].

Fig. 10 shows the neutron yield as a function of the pinch current and the pressure calculated with the model for the present experiment. It can be seen that the neutron yield at the optimum pressure follows a general trend represented by $I_p/(r_1\sqrt{p}) = 91$ kA/cm mbar$^{1/2}$ (solid curve in the figure). The dashed curve corresponds to $I_p/(r_1\sqrt{p}) = 77$ kA/cm mbar$^{1/2}$. The maximum neutron yield is achieved at the top of the graphic for $I_p = I_{\max}$. From this perspective, (16) can be interpreted as a physical basis of the drive parameter. Moreover, (16) associates the drive parameter with the pinch reactive fraction ξ_R.

The present model can be applied to analyze the sensibility of the neutron production of small PF devices to different design parameters. As an example, Fig. 11 shows how the region of maximum neutron yield changes when varying the anode radius. The central region corresponds to the experimental device described in Section II. Increasing the anode radius the maximum yield moves to lower pressures, and vice versa, as it is expected to keep the driver parameter within the optimum range. In the three shown regions (for anode radii 2.5, 3, and 3.5 mm) the latter remains between

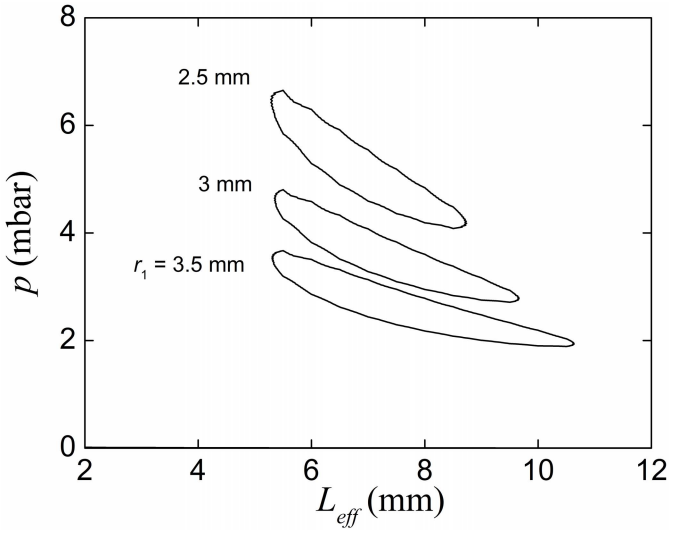

Fig. 11. Position of the region of maximum neutron yield for different anode radii. Inside each region the driver parameter remains in its optimum range.

74 and 94 kA/cm mbar$^{1/2}$, being 91 kA/cm mbar$^{1/2}$ in the center of each region.

V. Conclusion

A semiempirical model of the PF operation and neutron emission was formulated generalizing previous versions of lumped-parameter models. The model was validated with experimental data from a small PF device of 50 J with four different anodes, reporting the neutron yield together with the electrical diagnostics. Good agreement with the experiment was found, especially regarding the dependence of the neutron yield with the pressure and anode length.

The relation of the neutron yield with the pinch current showed a general agreement, which presents a trend that can be associated with the invariance of the driver parameter $I_p/(r_1\sqrt{p})$, commonly used in PF design [2]. The correlation found for the driver parameter given by (16) suggests that the natural dimensionless group for the physical mechanisms associated to this parameter is $\mu_o I_{\max}^2/r_1^2 p$. In the present case, 91 kA/cm mbar$^{1/2}$ corresponds to $\mu_o I_{\max}^2/r_1^2 p = 10^6$. There is a number of scaling laws that have been suggested elsewhere regarding the invariance of the driver parameter [2], [7]. The present results can shed some light on the interpretation of those laws.

The relation found between the driver parameter and ξ_R deserves some discussion. As is defined in (14), ξ_R can be interpreted as the fraction of deuterons initially contained in a cylinder of length h and radius r_1 that effectively contributes to the reaction process in the pinch. Interferometric measurements of the electron density performed in the device PF-50 J indicate that the mass trapped in the pinch is ~25% of the mass initially contained in the cylindrical volume [18]. Hence, the calibrated value $\xi_R \sim 0.01$ suggests that only ~4% of the deuterons of the pinch contributes to the reaction. Such a small fraction could be interpreted in various ways. It could be an indication of Taylor instabilities that produce hot spots in the pinch column where the reaction takes place. However, although this phenomenon has been reported in PF devices [41], it was not observed in the photographs and interferograms in PF-50 J. Another conjecture is that the reactions take place in a small central region of the pinch where the temperature is higher due to the sudden deceleration of the radial front. Nevertheless, it is stressed that this conclusion should be taken as a preliminary conjecture that requires further confirmation.

References

[1] L. Soto, "New trends and future perspectives on plasma focus research," *Plasma Phys. Controlled Fusion*, vol. 47, no. 5A, p. A361, 2005.
[2] L. Soto, C. Pavez, A. Tarifeño, J. Moreno, and F. Veloso, "Studies on scalability and scaling laws for the plasma focus: Similarities and differences in devices from 1 MJ to 0.1 J," *Plasma Sour. Sci. Technol.*, vol. 19, no. 5, p. 055017, 2010.
[3] D. Klir *et al.*, "Experimental evidence of thermonuclear neutrons in a modified plasma focus," *App. Phys. Lett.*, vol. 98, no. 7, p. 071501, 2011.
[4] P. Kubes, J. Kravarik, D. Klir, J. Kortanek, and K. Rezac, "Neutron production from a small modified plasma focus device," *IEEE Trans. Plasma Sci.*, vol. 40, no. 12, pp. 3298–3302, Dec. 2012.
[5] H. Bruzzone, M. O. Barbaglia, H. Nestor Acuna, M. M. Milanese, R. L. Moroso, and S. Guichon, "On probable fusion mechanisms in a Mather-type plasma focus," *IEEE Trans. Plasma Sci.*, vol. 41, no. 11, pp. 3180–3183, Nov. 2013.
[6] S. Lee, S. H. Saw, L. Soto, S. V. Springham, and S. P. Moo, "Numerical experiments on plasma focus neutron yield versus pressure compared with laboratory experiments," *Plasma Phys. Controlled Fusion*, vol. 51, no. 7, p. 075006, 2009.
[7] D. Klir and L. Soto, "Drive parameter of neutron-optimized dense plasma foci," *IEEE Trans. Plasma Sci.*, vol. 40, no. 12, pp. 3273–3279, Dec. 2012.
[8] P. Silva *et al.*, "A plasma focus driven by a capacitor bank of tens of joules," *Rev. Sci. Instrum.*, vol. 73, no. 7, pp. 2583–2587, 2002.
[9] J. Moreno, P. Silva, and L. Soto, "Optical observations of the plasma motion in a fast plasma focus operating at 50 J," *Plasma Sour. Sci. Technol.*, vol. 12, no. 1, p. 39, 2003.
[10] P. Silva, J. Moreno, L. Soto, L. Birstein, R. Mayer, and W. Kies, "Neutron emission from a fast plasma focus of 400 joules," *App. Phys. Lett.*, vol. 83, no. 16, pp. 3269–3271, Oct. 2003.
[11] P. Silva, L. Soto, W. Kies, and J. Moreno, "Pinch evidence in a fast and small plasma focus of only tens of joules," *Plasma Sour. Sci. Technol.*, vol. 13, no. 2, p. 329, 2004.
[12] L. Soto *et al.*, "Demonstration of neutron production in a table-top pinch plasma focus device operating at only tens of joules," *J. Phys. D, Appl. Phys.*, vol. 41, no. 20, p. 205215, 2008.
[13] L. Soto, C. Pavez, J. Moreno, M. Barbaglia, and A. Clausse, "Nanofocus: An ultra-miniature dense pinch plasma focus device with submillimetric anode operating at 0.1 J," *Plasma Sour. Sci. Technol.*, vol. 18, p. 015007, Nov. 2009.
[14] M. Milanese, R. Moroso, and J. Pouzo, "D-D neutron yield in the 125 J dense plasma focus nanofocus," *Eur. Phys. J. D, Atomic, Molecular, Opt., Plasma Phys.*, vol. 27, no. 1, pp. 77–81, 2003.
[15] R. K. Rout, P. Mishra, A. M. Rawool, L. V. Kulkarani, and S. C. Gupta, "Battery powered tabletop pulsed neutron source based on a sealed miniature plasma focus device," *J. Phys. D, Appl. Phys.*, vol. 41, no. 20, p. 205211, 2008.
[16] R. Verma, R. S. Rawat, P. Lee, M. Krishnan, S. V. Springham, and T. L. Tan, "Experimental study of neutron emission characteristics in a compact sub-kilojoule range miniature plasma focus device," *Plasma Phys. Controlled Fusion*, vol. 51, no. 7, p. 075008, 2009.
[17] M. Barbaglia, H. Bruzzone, H. Acuña, L. Soto, and A. Clausse, "Experimental study of the hard X-ray emissions in a plasma focus of hundreds of joules," *Plasma Phys. Controlled Fusion*, vol. 51, no. 4, p. 045001, 2009.
[18] A. Tarifeño-Saldivia, C. Pavez, J. Moreno, and L. Soto, "Dynamics and density measurements in a small plasma focus of tens-of-joules-emitting neutrons," *IEEE Trans. Plasma Sci.*, vol. 39, no. 2, pp. 756–760, Feb. 2011.
[19] A. Marquez, J. Gonzalez, A. Tarifeño-Saldivia, C. Pavez, L. Soto, and A. Clausse, "Modelling of the internal dynamics and density in a tens of joules plasma focus device," *Phys. Plasmas*, vol. 19, no. 1, p. 012703, 2012.
[20] A. Tarifeño-Saldivia and L. Soto, "Statistical characterization of the reproducibility of neutron emission of small plasma focus devices," *Phys. Plasmas*, vol. 19, no. 9, p. 092512, 2012.

[21] C. Pavez *et al.*, "Potentiality of a small and fast dense plasma focus as hard X-ray source for radiographic applications," *Plasma Phys. Controlled Fusion*, vol. 54, no. 10, p. 105018, 2012.
[22] M. Barbaglia, L. Soto, and A. Clausse, "Dependence of hard X-ray emissions with the charging pressure in a small plasma focus," *J. Fusion Energy*, vol. 31, no. 2, pp. 105–108, 2012.
[23] C. Moreno *et al.*, "Industrial applications of plasma focus radiation," *Brazilian J. Phys.*, vol. 32, no. 1, pp. 20–25, 2002.
[24] M. Zakaullah, K. Alamgir, M. Shafiq, M. Sharif A. Waheed, and G. Murtaza, "Low-energy plasma focus as a tailored X-ray source," *J. Fusion Energy*, vol. 19, no. 2, pp. 143–157, 2000.
[25] C. Pavez and L. Soto, "Demonstration of X-ray emission from an ultra-miniature pinch plasma focus discharge operating at 0.1 J nanofocus," *IEEE Trans. Plasma Sci.*, vol. 38, no. 5, pp. 1132–1135, May 2010.
[26] S. Hussain, S. Ahmad, M. Z. Khan, M. Zakaullah, and A. Waheed, "Plasma focus as a high intensity flash X-ray source for biological radiography," *J. Fusion Energy*, vol. 22, no. 3, pp. 195–200, 2004.
[27] S. Lee *et al.*, "High rep rate high performance plasma focus as a powerful radiation source," *IEEE Trans. Plasma Sci.*, vol. 26, no. 4, pp. 1119–1126, Aug. 1998.
[28] C. Moreno, A. Clausse, J. F. Martinez, R. Llovera, and A. Tartaglione, "Ultrafast X-ray introspective imaging of metallic objects using a plasma focus," *Nukleonika*, vol. 46, no. 1, pp. S33–S34, 2001.
[29] M. Venere, C. Moreno, A. Clausse, R. Barbuzza, and G. Del Fresno, "Tomographic system based on plasma focus X-rays," *Nukleonica*, vol. 46, no. 1, pp. S93–S94, 2001.
[30] V. Raspa *et al.*, "Plasma Focus as a powerful hard X-ray source for ultrafast introspective imaging of moving metallic objects," *Brazilian J. Phys.*, vol. 34, no. 4B, pp. 1696–1699, 2004.
[31] V. Raspa, C. Moreno, L. Sigaut, and A. Clausse, "Effective hard X-ray spectrum of a tabletop Mather-type plasma focus optimized for flash radiography of metallic objects," *J. Appl. Phys.*, vol. 102, no. 12, pp. 123303-1–123303-5, Jun. 2007.
[32] A. Tartaglione, R. Ramos, J. González, A. Clausse, and C. Moreno, "Detection of water by neutron scattering using a small plasma focus," *Brazilian J. Phys.*, vol. 34, no. 4B, pp. 1756–1758, 2004.
[33] J. L. Ellsworth *et al.*, "Design and initial results from a kilojoule level dense plasma focus with hollow anode and cylindrically symmetric gas puff," *Rev. Sci. Instrum.*, vol. 85, no. 1, p. 013504, 2014.
[34] V. A. Gribkov *et al.*, "A dense plasma focus-based neutron source for a single-shot detection of illicit materials and explosives by a nanosecond neutron pulse," *Phys. Scripta*, vol. 81, no. 3, p. 035502, 2010.
[35] J. T. Scheuer *et al.*, "A magnetically-nozzled, quasi-steady, multimegawatt, coaxial plasma thruster," *IEEE Trans. Plasma Sci.*, vol. 22, no. 6, pp. 1015–1033, Dec. 2001.
[36] M. Bhuyan, S. R. Mohanty, C. V. S. Rao, P. A. Rayjada, and P. M. Raole, "Plasma focus assisted damage studies on tungsten," *Appl. Surf. Sci.*, vol. 264, pp. 674–680, Jan. 2013.
[37] R. S. Rawat, "High-energy-density pinch plasma: A unique nonconventional tool for plasma nanotechnology," *IEEE Trans. Plasma Sci.*, vol. 41, no. 4, pp. 701–715, Apr. 2013.
[38] F. Casanova, A. Tarifeño-Saldivia, F. Veloso, C. Pavez, A. Clausse, and L. Soto, "Toroidal high-density singularity in a small plasma focus," *J. Fusion Energy*, vol. 31, no. 3, pp. 279–283, 2012.
[39] J. Moreno, L. Birstein, R. E. Mayer, P. Silva, and L. Soto, "System for measurement of low yield neutron pulses from D–D fusion reactions based upon a ^{3}He proportional counter," *Meas. Sci. Technol.*, vol. 19, no. 8, p. 087002, 2008.
[40] A. Tarifeño-Saldivia, R. E. Mayer, C. Pavez, and L. Soto, "Calibration methodology for proportional counters applied to yield measurements of a neutron burst," *Rev. Sci. Instrum.*, vol. 85, no. 1, pp. 013502-1–013502-9, Jan. 2014.
[41] L. Bilbao and H. Bruzzone, "Instability of the current sheath in plasma focus devices," *Phys. Lett. A*, vol. 101, nos. 5–6, pp. 261–262, 1984.
[42] A. Clausse, L. Bilbao, and H. Bruzzone, "Engineering basis for thermonuclear pulsed neutron generators," *J. Tech. Phys.*, vol. 39, pp. 33–37, 1998.
[43] C. Moreno, H. Bruzzone, J. Martínez, and A. Clausse, "Conceptual engineering of plasma-focus thermonuclear pulsors," *IEEE Trans. Plasma Sci.*, vol. 28, no. 5, pp. 1735–1741, Oct. 2000.
[44] C. Moreno, F. Casanova, G. Correa, and A. Clausse, "Experimental study and two-dimensional modelling of the plasma dynamics of magnetically driven shock waves in a coaxial tube," *Plasma Phys. Controlled Fusion*, vol. 45, no. 12, pp. 1989–1999, 2003.
[45] F. Casanova, C. Moreno, and A. Clausse, "Finite-elements numerical model of the current-sheet movement and shaping in coaxial discharges," *Plasma Phys. Controlled Fusion*, vol. 47, no. 8, pp. 1239–1250, 2005.
[46] A. Tarifeño-Saldivia, "Estudio experimental de una descarga plasma focus rapida operada en el rango de decenas de joules emitiendo neutrones," Ph.D. dissertation, Facultad de Ciencias Físicas y Matemáticas, Universidad de Concepción, Concepción, Chile, Jan. 2011.
[47] F. N. Beg, M. Zakaullah, M. Nisar, and G. Murtaza, "Role of anode length in a Mather-type plasma focus," *Modern Phys. Lett. B*, vol. 6, no. 10, pp. 593–597, 1992.
[48] J. H. González, A. Clausse, H. Bruzzone, and P. C. Florido, "A lumped parameter model of plasma focus," *IEEE Trans. Plasma Sci.*, vol. 32, no. 3, pp. 1383–1391, Jun. 2004.
[49] J. H. González, F. R. Brollo, and A. Clausse, "Modeling of the dynamic plasma pinch in plasma focus discharges based in Von Karman approximations," *IEEE Trans. Plasma Sci.*, vol. 37, no. 11, pp. 2178–2185, Nov. 2009.

Alejandro Clausse was born in Buenos Aires, Argentina, in 1957. He received the master's and Ph.D. degrees in nuclear engineering from the Balseiro Institute, Bariloche, Argentina, in 1981 and 1987, respectively.

He is currently a Professor of Engineering with the National University of Central Buenos Aires, Tandil, Argentina. He heads the Department of Dense Plasmas with the National Atomic Energy Commission, and is a Principal Researcher with the National Science and Technology Council of Argentina. His current research interests include advanced nuclear reactors and physics of fluids and plasmas.

Leopoldo Soto received the B.S., M.S., and Ph.D. degrees in physics from the Pontificia Universidad Católica de Chile, Santiago, Chile, in 1989, 1990, and 1993, respectively.

He is the Head of the Department of Thermonuclear Plasma, Nuclear Chilean Energy Commission (CCHEN), and the Director of the Center for Research and Applications in Plasma Physics and Pulsed Power, P4 CCHEN, University of Talca, Talca, Chile. He is an Associate Professor of the Ph.D. Program in Physics with the University of Concepción, Concepción, Chile, and the Ph.D. Program in Applied Science, University of Talca, and an Associate Full Professor with the Departamento de Ciencias Físicas, Universidad Andres Bello, Santiago, Chile. His current research interests include dense transient plasmas, pulsed power and applied optics, including Z-pinch, plasma focus, nuclear fusion mechanisms, capillary discharges, pulsed power miniature devices, effects of pulsed radiation on materials and on biological objects, transient plasma diagnostics, holography, interferometry, and optical refractive diagnostics.

Dr. Soto was elected as fellow of the Institute of Physics, U.K., in 2007. He was a recipient of the Presidential Chair in Science by the President of Chile in 1999. He was the President of the Chilean Physical Society for two periods from 2003 to 2008. He will be the Secretary General of the Chilean Physical Society from 2013 to 2015.

Ariel Tarifeño-Saldivia was born in Santiago, Chile, in 1982. He received the B.S. degree in physics from the Universidad de Chile, Santiago, in 2004, and the Ph.D. degree in physics from the Universidad de Concepción, Concepción, Chile, in 2011.

He was a Graduate and Post-Doctoral Researcher with the Chilean Nuclear Energy Commission, where he focused on plasma dynamics and neutron emissions of tabletop plasma focus devices, neutron detection, and Monte Carlo modeling. He is currently a Post-Doctoral Researcher with the Instituto de Física Corpuscular Valence, Spain. His current research interests include experimental nuclear physics, neutron detection and advanced nuclear instrumentation for experiments on beta-delayed neutrons, background measurements in underground laboratories, measurements of neutron cross-sections for astrophysics and nuclear technology, and experiments in nuclear fusion devices.